VIII International Conference on Fracture Mechanics of Concrete and Concrete Structures
FraMCoS-8
J.G.M. Van Mier, G. Ruiz, C. Andrade, R.C. Yu and X.X. Zhang (Eds)

COUPLED ELASTO-PLASTIC MODEL WITH NON-LOCAL SOFTENING ENHANCED BY VISCOSITY TO DESCRIBE DYNAMIC CONCRETE BEHAVIOUR

I. MARZEC[*†] **AND J. TEJCHMAN**[†]

[†] Gdańsk University of Technology
Narutowicza 11/12, 80-952 Gdańsk, Poland
e-mail: irek@pg.gda.pl, tejchmk@pg.gda.pl

Key words: Concrete, Elasto-plasticity, Non-local theory, Dynamic behaviour, Viscosity

Abstract: The paper presents results of FE simulations of the concrete behaviour under dynamic loading at the different strain-rate. A continuum elasto-plastic constitutive model was used. Viscosity, non-locality and inertial terms were included. Numerical results of strength during uniaxial compression and uniaxial tension were compared with corresponding laboratory tests and CEB recommendations. Some preliminary own dynamic test results on concrete beams under three-point bending were also shown.

1 INTRODUCTION

A fracture process is a fundamental phenomenon in quasi-brittle materials like concrete [1]. It is subdivided in general into 2 main stages: appearance of narrow regions of intense strain deformation with a certain width (including micro-cracks) and occurrence of macro-cracks. Within continuum mechanics, strain localization can be numerically captured by a continuous approach and discrete macro-cracks by a discontinuous one. Usually, to describe the fracture behaviour of concrete, one approach is used. However, in order to describe the entire fracture process, a continuous approach should be connected with a discontinuous one [2]. Fracture and strength strongly depends among others on the loading velocity. The structural concrete resistance increases when the strain rate increases ([3]-[6]) due to 2 main reasons: inertia forces of micro-cracking and viscosity of free water in the capillary concrete system ([4], [5]). The concrete behaviour at high strain rates is also strongly influenced by fragmentation [7]. Thus, concrete is a highly rate-dependent material ([8]-[10]).

Two different phases in the strength increase can be distinguished in compression and tension (Figs.1 and 2). Under compression, the first phase corresponds to the strain rate $\dot{\varepsilon} < 10^{-1}$ 1/s (it leads to the maximum 1.5-times increase of the compressive strength) and the second one $\dot{\varepsilon} \geq 10^{-1}$ 1/s (it leads to the maximum 3-times increase of the compressive strength). Under tension two distinct phases happen in the increase of the tensile strength. At $\dot{\varepsilon} = 10^{0}$ 1/s the tensile strength is 2-times higher and at $\dot{\varepsilon} = 10^{2}$ 1/s is even 9-times greater.

The aim of our research is to formulate a reliable continuum constitutive model for describing the concrete behaviour under dynamic conditions verified by experimental dynamic results.

Initial FE calculations were carried out with a coupled elasto-plastic-damage continuum model with non-local softening to capture a quasi-static cyclic behaviour of concrete [11]. Next, the concrete dynamic behaviour was simulated with an elasto-plastic model

enhanced by usual viscosity. The viscosity was incorporated via the Duvaut–Lions approach which allows for coupling of different criteria (in contrast to the Perzyna model). To properly reproduce strain localization, in particular for small loading velocities, non-local terms were also introduced into a constitutive formulation during softening.

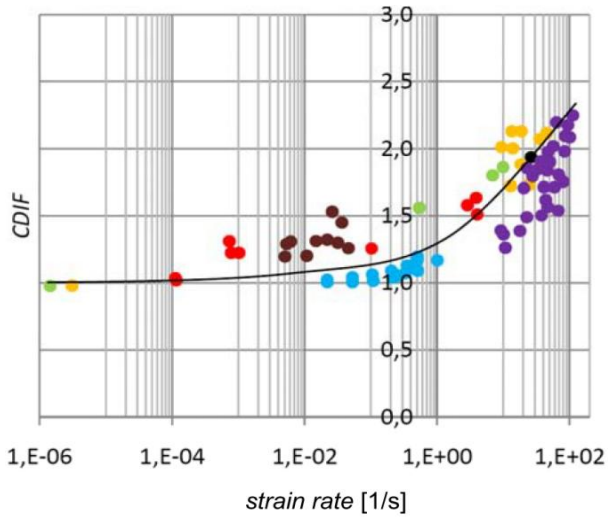

Figure 1: Increase of concrete strength versus strain rate during compression from different laboratory test [9] (CDIF – compressive dynamic increase factor).

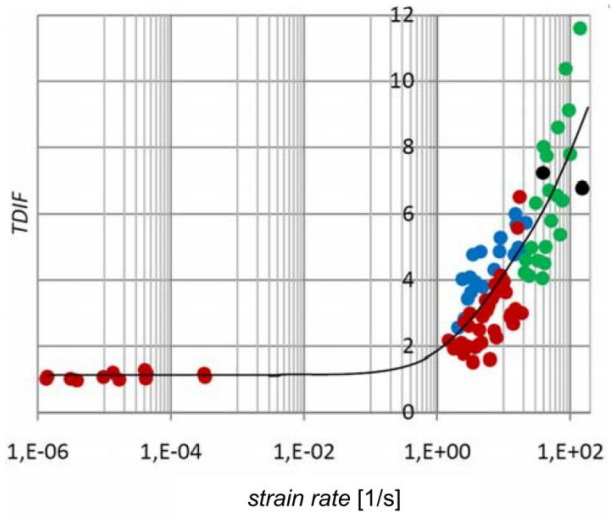

Figure 2: Increase of concrete strength versus strain rate during tension from different laboratory test [9] (TDIF – tensile dynamic increase factor).

2 MODEL FOR CONCRETE UNDER DYNAMIC CONDITIONS

Our elastic-visco-plastic continuum concrete model was developed based on the rate-independent elasto-plastic formulation enhanced by viscosity incorporated via the so-called Duvaut–Lions over-stress approach [12], wherein the stress state is allowed to remain outside the yield surface.

To describe inviscid behaviour, the Drucker-Prager criterion in compression and the Rankine criterion in tension were assumed. In a compression regime, a shear yield surface based on the linear Drucker-Prager criterion with isotropic hardening and softening was used [13]

$$f_1 = q + p\tan\varphi - \left(1 - \frac{1}{3}\tan\varphi\right)\sigma_c\left(\kappa_1\right), \qquad (1)$$

where q is the Mises equivalent deviatoric stress, p denotes the mean stress and φ is the internal friction angle. The evolution of material hardening/softening was defined by the uniaxial compression yield stress $\sigma_c(\kappa_1)$. The internal friction angle φ was assumed as

$$\tan\varphi = \frac{3\left(1 - r_{bc}^{\sigma}\right)}{1 - 2r_{bc}^{\sigma}}, \qquad (2)$$

where $r_{bc}{}^{\sigma}$ is the ratio between the biaxial compressive strength and uniaxial compressive strength ($r_{bc}{}^{\sigma}$=1.2). The invariants q and p are

$$q = \sqrt{\frac{3}{2}s_{ij}s_{ji}} \quad \text{and} \quad p = \frac{1}{3}\,\sigma_{kk}, \qquad (3)$$

where σ_{ij} is the stress tensor and s_{ij} denotes the deviatoric stress tensor. The flow potential was defined as

$$g_1 = q + p\tan\psi, \qquad (4)$$

where ψ is the dilatancy angle ($\psi \neq \varphi$). For the sake of simplicity, the constant values of φ and ψ were assumed. In turn, in a tensile regime, a Rankine criterion was used with a yield function f_2 with isotropic softening defined as [13]

$$f_2 = \max\{\sigma_1, \sigma_2, \sigma_3\} - \sigma_t\left(\kappa_2\right), \qquad (5)$$

where σ_i – the principal stress, $\sigma_t(\kappa_2)$ – the tensile yield stress and κ_2 – the softening parameter equal to the maximum principal plastic strain. The associated flow rule was assumed. The edges and vertex in Rankine yield function were taken into account by the interpolation of 2-3 plastic multipliers according to the Koiter's rule. The same procedure was adopted in the case of combined tension (Rankine criterion) and compression (Drucker-Prager criterion). This inviscid isotropic elasto-plastic model for concrete (Eqs.1-5) requires two elastic parameters: modulus of elasticity E and Poisson's ratio υ, one compression yield stress function $\sigma_c=f(\kappa_1)$ (based on a uniaxial compression test), one tensile yield stress function $\sigma_t=f(\kappa_2)$ (based on a uniaxial tension test), internal friction angle φ and dilatancy angle ψ (based on a triaxial compression test). The model has some simplifications. The shape of the failure surface in a principal stress space is linear (not paraboloidal as in reality). In deviatoric planes, the shape is circular (during compression) and triangular (during tension); thus it does not gradually change from a curvilinear triangle with smoothly rounded corners to nearly circular with increasing pressure. The strength is similar for triaxial compression and extension, and the stiffness degradation due to strain localization and non-linear volume changes during loading are not taken into account.

The viscosity was incorporated based on the Duvant-Lions approach, wherein a viscoplastic solution was simply constructed through the relevant plastic solution. The biggest advantage of this approach is the easy numerical implementation (only an additional simple stress update loop is needed in existing elasto-plastic algorithms). The visco-plastic strain rate and hardening parameter were respectively defined as

$$\dot{\varepsilon}_{ij}^{vp} = \frac{1}{\tau}\left[C_{ijkl}^{e}\right]^{-1}\left(\sigma_{kl}-\bar{\sigma}_{kl}\right), \tag{6}$$

$$\dot{\kappa}^{vp} = \frac{1}{\tau}\left(\kappa-\bar{\kappa}\right), \tag{7}$$

where τ is the material parameter usually called the relaxation time, and are the stress and hardening/softening parameter of an inviscid material. The visco-plastic strain rate (Eq.6) was defined by the difference between the true stresses and stresses obtained in an inviscid material. The total strain rate partition into an elastic strain rate and a visco-plastic strain rate was assumed

$$\dot{\varepsilon}_{ij} = \dot{\varepsilon}_{ij}^{e} + \dot{\varepsilon}_{ij}^{vp}. \tag{8}$$

Such formulation allows for a smooth transition from an inviscid to viscous case (in contrast to the Perzyna visco-plastic model). The material was initially considered to be as a rate independent one, so the plastic stress tensor and a hardening variable were obtained. Later, the rate-dependency was incorporated by means of Eqs.6 and 7. After solving Eqs.6 and 7, one obtained the updated viscoplastic stress and the updated viscoplastic softening parameter integrated over the time step Δt (from t to $t+\Delta t$)

$$\sigma_{ij}^{n+1} = \frac{\left(\sigma_{ij}^{n} + \boldsymbol{C}_{ijkl}^{e} : \Delta\boldsymbol{\varepsilon}_{kl}\right) + \dfrac{\Delta t}{\tau}\bar{\sigma}_{ij}^{n+1}}{1+\dfrac{\Delta t}{\tau}}, \tag{9}$$

$$\kappa_{n+1} = \frac{\kappa_n + \dfrac{\Delta t}{\tau}\bar{\kappa}_{n+1}}{1+\dfrac{\Delta t}{\tau}}. \tag{10}$$

A Duvant-Lions visco-plastic model is quite convenient to be implemented, since a visco-plastic solution is the update of the inviscid solution [8]. A Duvant-Lions visco-plasticity produces a length in field equations as a multiplication product of the elastic wave speed times the relaxation time [12].

3 MODELLING OF STRAIN LOCALIZATION

An integral-type non-local theory was used as a regularization technique to describe strain localization at the entire strain rate range ([14], [15], [16]). It takes advantage of a weighted

spatial averaging of a suitable state variable over a neighbourhood of each material point. Thus, a state variable at a certain material point depends not only on the state variable at the point but on the distribution of the state variable in a finite neighbourhood of the point considered (the principle of a local action does not hold – a non-local interaction takes place between any two points). It has a physical motivation due to the fact the distribution of stresses in the interior of concrete at meso-scale is strongly non-uniform due to the presence of different phases (aggregate, cement, bond). Usually, in elasto-plastic formulations, it is sufficient to achieve mesh-independent FE results to treat non-locally one state variable controlling material softening (e.g. non-local softening parameter), whereas stresses, strains and other variables remain local ([15], [17]).

In the case of dynamic problem, the viscosity solution is an appropriate solution to regularize the initial value problem. However for quasi-static this approach is not sufficient. The non-locality was introduced into the constitutive formulation in an inviscid phase of the model. The rates of the inviscid softening parameter (Eq.7) were averaged according to Brinkgreve [15]

$$\mathrm{d}\tilde{\kappa}_i(\boldsymbol{x}) = \mathrm{d}\bar{\kappa}_i(\boldsymbol{x}) + \\ + m\left(\int \omega(\boldsymbol{x},\boldsymbol{\xi})\,\mathrm{d}\bar{\kappa}_i(\boldsymbol{\xi})\,\mathrm{d}\boldsymbol{\xi} - \mathrm{d}\bar{\kappa}_i(\boldsymbol{x})\right), \quad (11)$$

Since the rate of the softening parameter is not known at the iteration beginning, some extra sub-iterations are required to solve Eq.11. To simplify the calculations, the non-local rates were replaced by their approximations $d\bar{\kappa}_i^{est}$ calculated based on the known total strain rate [15]

$$\mathrm{d}\tilde{\kappa}_i(\boldsymbol{x}) \approx \mathrm{d}\bar{\kappa}_i(\boldsymbol{x}) + \\ + m\left(\int \omega(\boldsymbol{x},\boldsymbol{\xi})\,\mathrm{d}\bar{\kappa}_i^{est}(\boldsymbol{\xi})\,\mathrm{d}\boldsymbol{\xi} - \mathrm{d}\bar{\kappa}_i^{est}(\boldsymbol{x})\right). \quad (12)$$

The FE results show an insignificant influence of the calculation method of plastic rates of the non-local softening parameter [17]. In addition, an approximate method proposed by Brinkgreve [15] in Eq.12 is less time consuming (by ca.30%).

As a weighting function ω (called also an attenuation function or a non-local averaging function), the Gauss distribution was assumed [16] independently of strain rates

$$\omega(r) = \frac{1}{c_g} e^{-\left(\frac{r}{l_c}\right)^2}, \quad (13)$$

where the parameter l_c is the characteristic length of micro-structure, r is the distance between two material points and cg denotes the normalizing factor equal to $\sqrt{\pi} l_c$ (1D case), πl_c^2 (2D case) and $\pi\sqrt{\pi} l_c^3$ (3D case). The averaging in Eq.13 is restricted to a small representative area around each material point (the influence of points at the distance of r=3×l_c is only of 0.01%). The weighting function satisfies the normalizing condition [16].

$$\omega(x,\xi) = \frac{\omega_0\left(\|x-\xi\|\right)}{\int_V \omega_0\left(\|x-\zeta\|\right)\mathrm{d}\zeta}. \quad (14)$$

A characteristic length is usually related to the micro-structure of concrete represented by the aggregate size. Based on our both numerical simulations of concrete and reinforced concrete beams under bending and experiments using a digital image correlation DIC technique in order to measure the width of a localized zone on the concrete surface, a characteristic length l_c of micro-structure was about 5 mm in usual concrete (using the Gauss distribution function). A proper non-local transformation requires that a non-local field corresponding to a constant local field remains constant in the vicinity of a boundary.

The models where implemented into the Abaqus Standard program with the aid of the subroutine UMAT (user constitutive law definition) and UEL (user element definition). For the solution of a non-linear equation of motion governing the response of a system of finite elements, a modified Newton-Raphson scheme (for simulation neglecting inertia effects) and Newmark algorithm (for simulation including inertia effects) were used. The calculations were performed with a symmetric elastic global stiffness matrix

instead of applying a tangent stiffness matrix (the choice was governed by access limitations in the commercial software Abaqus). The procedure yielded sufficiently accurate and fast convergence. The magnitude of the maximum out-of-balance force at the end of each calculation step was smaller than 1% of the calculated total force on the specimen. To satisfy the consistency condition f=0 in elasto-plasticity, the trial stress method (linearized expansion of the yield condition about the trial stress point) using an elastic predictor and a plastic corrector with the return mapping algorithm was applied. The calculations were carried out using a large-displacement analysis. In this case, the actual configuration of the body is taken into account. The Cauchy stress was taken as the stress measure. The conjugate strain rate was the rate of deformation. The rotation of the stress and strain tensor was calculated with the Hughes-Winget method. A non-local averaging was performed in the current configuration. This choice was governed by the fact that element areas in this configuration were automatically calculated by Abaqus.

4 FE RESULTS FOR DYNAMIC TESTS

In order to investigate the ability of presented formulation to proper reproduce the strengthening effect under both dynamic tension and compression initially the attention was laid on influence of viscosity and inertial forces on the strength. Therefore, the material constants (in particular the relaxation time τ) were taken in FE analyses in order to satisfactorily match numerical results with experimental ones.

4.1 Uniaxial compression test

A cube specimen was fixed at the lower and upper surfaces and the uniform vertical displacement was imposed along the upper boundary in the range 0-1 mm (Fig.3). The basic concrete parameters were: E=37.7 GPa, ν=0.15, ϕ=14º, ψ=8º, the compressive yield stress σ_{yc0}=30 MPa with linear softening (H=1.55 GPa). The relaxation time was equal to 1×10^{-6}, 2×10^{-6}, 1×10^{-5}, 2×10^{-5} and 2×10^{-4}. The calculations were performed as 2D (with plane strain triangular elements in the so called "union jack pattern") and 3D (with eight-node brick elements with full integration) (Fig.3).

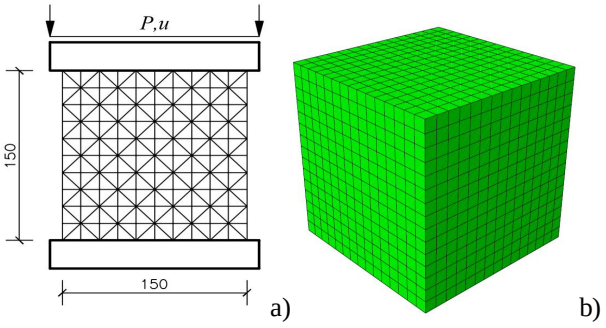

Figure 3: Uniaxial compression test for numerical calculations: a) specimen geometry with boundary conditions and b) mesh discretization.

The effect of several different loading strain rates ranged from 10^{-5} 1/s up to 10^{2} 1/s was investigated on the concrete dynamic behaviour. The numerical strength results were compared with the compressive dynamic increase factor (CDIF) according to the CEB recommendation [4].

First, the dynamic results using the visco-plastic model (simulation #1, $\tau=2\times10^{-5}$) and elasto-plastic model (simulation #2) with non-local softening (l_c=5 mm) were compared during 2D and 3D calculations (Fig.4). The calculated dynamic increase factor is underestimated as compared to CEB for the strain rate $\dot{\varepsilon}$ <1 1/s, since the same results were obtained for strain rates $\dot{\varepsilon}$ <1 1/s. In turn, for high strain rates ($\dot{\varepsilon}$ >10 1/s), the calculated dynamic increase factor is overestimated since fragmentation was not taken into account. The increase of CDIF is more pronounced in real 3D simulations than in simplified 2D analyses. In the case of viscous simulations, the increase factor CDIF obviously increases slightly faster than in non-viscous simulations for $\dot{\varepsilon}$ >10 1/s.

The influence of the viscous relaxation time τ is shown in Fig.5. The relaxation time varied between $\tau=1\times10^{-6}$ and $\tau=2\times10^{-4}$. The results show that an increase of the viscosity parameter leads to a faster growth of strength at loading rates $\dot{\varepsilon} \geq 10^{1}\ \left[1/\mathrm{s}\right]$ only. With large

relaxation, an increase of DIF was obtained also at $\dot{\varepsilon}$ ~1 1/s, but simultaneously it grew too rapidly at large strain rates.

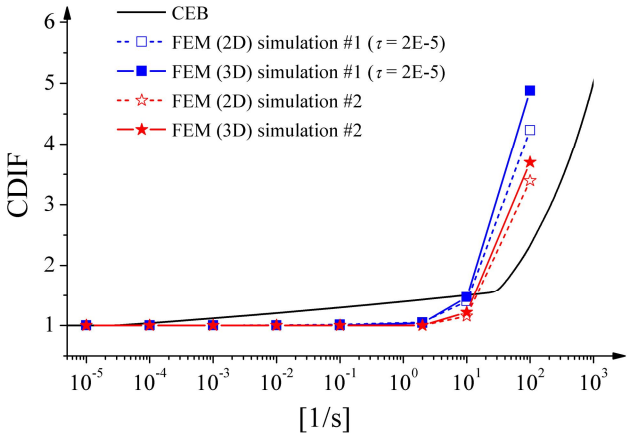

Figure 4: Dynamic FE simulation results considering effect of formulation type and presence of viscosity with relaxation time τ=2×10^{-5} as compared to dynamic compressive increase factor CDIF by CEB (#1 - elasto-visco-plastic model with non-local softening and #2 - elasto-plastic model with non-local softening).

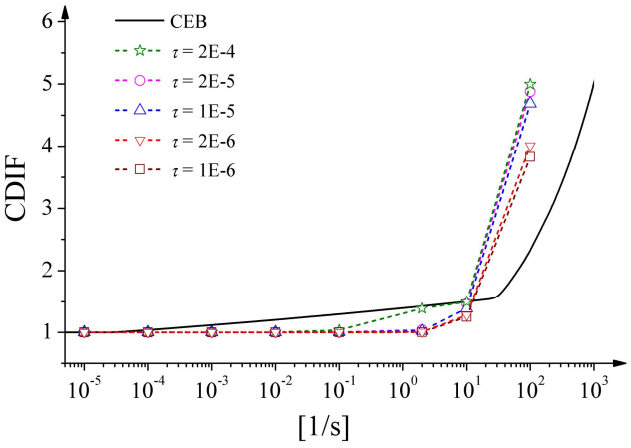

Figure 5: Dynamic FE results of CDIF with different relaxation time τ using elasto-visco-plastic model with non-local softening as compared to CEB curve.

4.2 Direct tension test

A dumbbell-shaped specimen was considered as in the experiments by Yan and Lin [18] (Fig.6). The following material parameters were assumed in FE calculations: E=29.0 GPa, ν=0.15 and the tensile yield stress σ_{yt0}=2 MPa with linear softening (H=0.65 GPa). The numerical dynamic simulations were performed with the strain rate varying between 10^{-5} 1/s and 10^{1} 1/s (the experiments were carried out at the loading strain rate ranged from 10^{-5} 1/s up to 10$^{-0.3}$ 1/s). The numerical results with the elasto-visco-plastic model with non-local softening (l_c=5 mm) and different viscosity parameter: τ=1×10^{-6}, 1×10^{-5}, 2×10^{-5}, 1×10^{-4} and 2×10^{-4} (simulation #1) were compared with those with the pure elasto-plastic model with non-local softening (l_c=5 mm) (simulation #2).

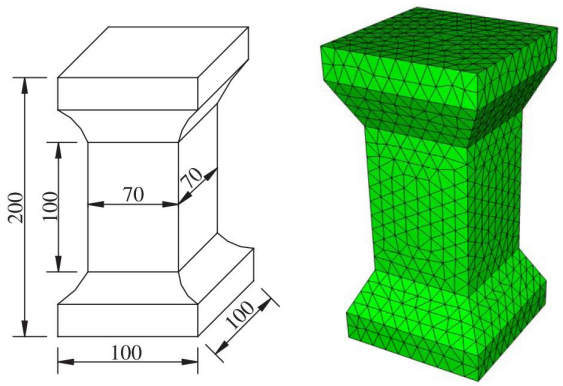

Figure 6: Uniaxial tension with of dumbbell-shaped concrete specimen: geometry [18] and FE mesh.

The summarized FE results are shown in Figs.7 and 8. Similarly as under compression, the numerical outcomes show that the dynamic increase factor is underestimated as compared to the both experiments [18] and CEB recommendation for the small strain rates $\dot{\varepsilon}$ <1 1/s) and overestimated for large strain rates. An increase of a viscosity parameter leads to a better accordance with the comparative data, however only at the strain rate $\dot{\varepsilon}$ <1 1/s. In turn, for the higher loading rates, the calculated dynamic effect is quite close to CEB for a very small viscosity parameter τ. For simulation #2 (without viscosity) the strength increase with increasing strain rate is practically not obtained. In the calculations, the softening rate increased with increasing strain rate at small strain rates and was similar at large strain rates.

5 OWN LABORATORY TESTS

In order to get a better insight into the concrete behaviour under dynamic loading, some experimental tests were conducted using

a servo-hydraulic load machine Zwick HB 250. The cyclic dynamic vertical force-displacement diagrams were measured over a wide range of loading rates (from 0.0005 mm/s up to 5 mm/s). The displacements on the concrete surface were registered using the Digital Image Correlation technique to register the shape and width of localization zones and cracks.

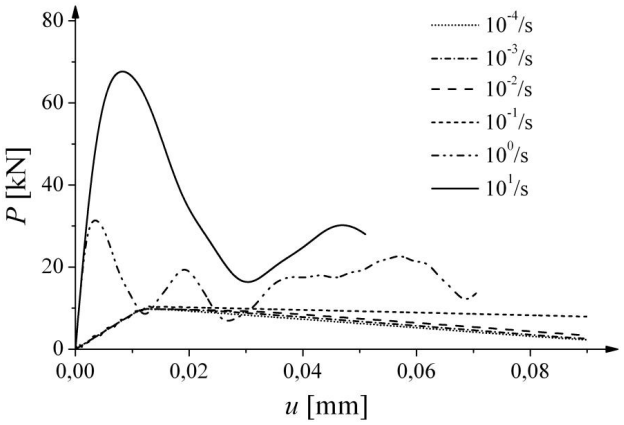

Figure 7: The load-displacement curves from FE dynamic simulations for different vertical strain rate using elasto-visco-plastic model with non-local softening (τ=2×10^{-5}, l_c=5 mm).

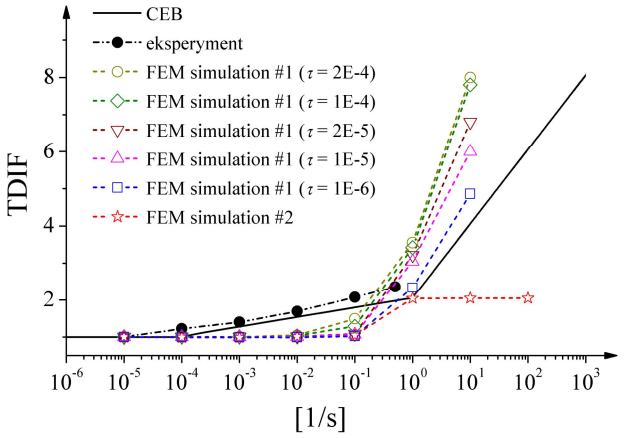

Figure 8: Dynamic FE results of uniaxial tension as compared to TDIF by CEB for different vertical strain rate at different relaxation times (#1 - elasto-visco-plastic model with non-local softening and #2 - elasto-plastic model with non-local softening).

The measured force-displacement evolutions are demonstrated in Fig.9. The strength and material brittleness increase with increasing strain rate.

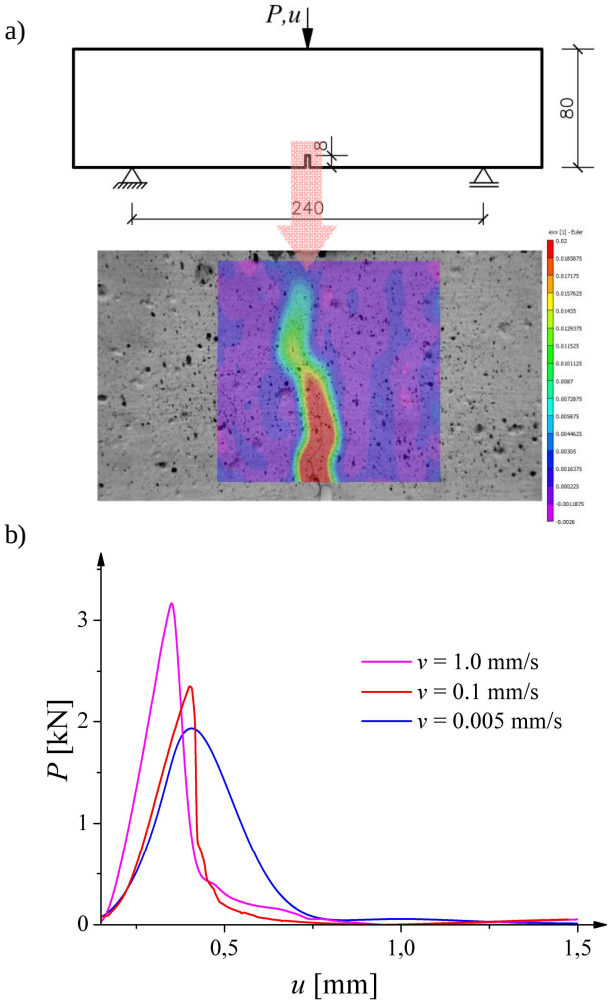

Figure 9: Results of own initial experimental dynamic tests on concrete beams under three-point bending: a) specimen geometry and contours of localized zone captured with DIC, b) force-displacement curves at different loading rate.

6 CONCLUSIONS

The FE calculations with the elasto-visco-plastic model with non-local softening show that at small loading strain rates, the calculated dynamic increase factor is too small and for high loading strain rates is too high as compared to the CEB recommendation. Thus, usual viscosity in a plastic domain is not a sufficient tool to realistically describe the concrete dynamic behaviour. Further research works are needed by taking into account elastic and retarding viscosity, and material fragmentation in the constitutive concrete formulation at macro-level.

REFERENCES

[1] Bažant, Z. P., Planas, J., 1998. *Fracture and size effect in concrete and other quasi-brittle materials*. CRC Press LLC.

[2] Moonen, P., Carmeliet, J., Sluys, L.J., 2008. A continuous-discontinuous approach to simulate fracture processes. *Philosophical Magazine* **88**:3281-3298.

[3] Bischoff, P. H., Perry, S. H., 1991. Compressive behavior of concrete at high strain rates, *Mat. Struct.* **24**:425-450.

[4] Javier Malvar, L., Crawford, J.E., 1998. Dynamic Increase factors for concrete, *Twenty-Eighth DDESB Seminar*, Orlando, FL.

[5] Zheng, D., Li, Q., 2004. An explanation for rate effect of concrete strength based on fracture toughness including free water viscosity, *Engineering Fracture Mechanics* **71**:2319-2327.

[6] Zhang, X.X., Ruiz, G., Yu, G. R.C., Tarifa, M., 2009. Fracture behaviour of high-strength concrete at a wide range of loading rates. *International Journal of Impact Engineering*, **36**:1204–1209.

[7] Werner, S., Thienel, K.-Ch., 2011. Influence of impact velocity on the fragment formation of concrete specimens. *Proc. Conference on Particles 2011*, Barcelona; pp. 211-221.

[8] Winnicki, A., 2007. *Viscoplastic and internal discontinuity models in analysis of structural concrete*. Habilitation, Cracow University of Technology.

[9] Pedersen, R.R., 2009. *Computational Modelling of Dynamic Failure of Cementitious Materials*. PhD Dissertation, TU Delft, the Netherlands.

[10] Häussler-Combe, U., Kuehn, T., 2012. Failure modelling of concrete with a novel strain rate sensitive viscoelastic retarded damage material formulation. *European Congress on Computational Methods in Applied Sciences and Engineering (ECCOMAS 2012)*, Vienna, Austria.

[11] Marzec I., Tejchman, J., 2012. Enhanced coupled elasto-plastic-damage models to describe concrete behaviour in cyclic laboratory tests: comparison and improvement. *Archives of Mechanics*, **64**, 3, pp. 227–259.

[12] Sluys, L.J., 1992. *Wave Propagation, Localization and Dispersion in Softening Solids*. PhD Thesis, Department of Civil Structural Engineering, Delft University of Technology, The Netherlands.

[13] Marzec, I., Bobinski, J. and Tejchman, J., 2007. Simulations of crack spacing in reinforced concrete beams using elastic-plasticity and damage with non-local softening. *Computers and Concrete* **4**(5):377-403.

[14] Pijaudier-Cabot, G. and Bažant, Z.P., 1987. Nonlocal damage theory. *ASCE J. Eng. Mech.*, **113**:1512-1533.

[15] Brinkgreve, R.B., 1994. *Geomaterial models and numerical analysis of softening*. PhD Thesis, Delft University of Technology, Delft.

[16] Bažant, Z.P., Jirásek, M., 2002. Nonlocal integral formulations of plasticity and damage: survey of progress. *J. Engng. Mech.*, **128**, 11; pp. 1119-1149.

[17] Bobiński, J., Tejchman, J., 2004. Numerical simulations of localization of deformation in quasi-brittle materials within non-local softening plasticity, *Computers and Concrete* **4**:433-455.

[18] Yan, D. and Lin, G., 2006. Dynamic properties of concrete in direct tension. *Cement and Concrete Research* **36**:1371-1378.